

# Information content of multiwavelength lidar data with respect to microphysical particle properties derived from eigenvalue analysis

Igor Veselovskii, Alexei Kolgotin, Detlef Müller, and David N. Whiteman

The multiwavelength Raman lidar technique in combination with sophisticated inversion algorithms has been recognized as a new tool for deriving information about the microphysical properties of atmospheric aerosols. The input optical parameter sets, provided by respective aerosol Raman lidars, are at the theoretical lower limit at which these inversion algorithms work properly. For that reason there is ongoing intense discussion of the accuracy of these inversion methods and the possibility of simultaneous retrieval of the particle size distribution and the complex refractive index. We present results of the eigenvalue analysis, used to study the information content of multiwavelength lidar data with respect to microphysical particle properties. Such an analysis provides, on a rather mathematical basis, more insight into the limitations of these inversion algorithms regarding the accuracy of the retrieved parameters. We show that the effective radius may be retrieved to 50% accuracy and the real and imaginary part of the complex refractive index to  $\pm 0.05$  and  $\pm 0.005i$ , if the imaginary part is  $< 0.02i$ . These results are in accordance with the classic approach of simulation studies with synthetic particle size distributions. Major difficulties are found with a particle effective radius of  $< 0.15 \mu\text{m}$ . In that case the complex refractive index may not be derived with sufficient accuracy. The eigenvalue analysis also shows that the accuracy of the derived parameters degrades if the imaginary part is  $> 0.02i$ . Furthermore it shows the importance of the simultaneous use of backscatter and extinction coefficients for the retrieval of microphysical parameters. © 2005 Optical Society of America

OCIS codes: 010.1100, 010.3640, 290.1090, 290.5860.

## 1. Introduction

In the past 15 years significant progress has been made toward the microphysical characterization of atmospheric particles with multiwavelength Raman lidar. The measured optical quantities in terms of backscatter and extinction coefficients are processed by an inversion algorithm into the microphysical properties of interest by using Tikhonov's inversion with regularization.<sup>1-3</sup> Starting from the exploratory theoretical work of Qing *et al.*,<sup>4</sup> it has been shown that the combined use of backscatter and extinction coefficients permits retrieving aerosol size distribu-

tion parameters with rather high accuracy.<sup>5-10</sup> Moreover this technique of data combination also allows an estimation of the particle complex refractive index. This result is particularly important in view of the fact that the vertically resolved single-scattering albedo can be derived for ambient atmospheric conditions.<sup>11</sup>

The results of Müller *et al.*<sup>5-7</sup> were based on data sets provided by a unique six-wavelength aerosol Raman lidar,<sup>12</sup> specifically designed to explore the potential of the particle characterization with lidar. It soon became clear that the costs and required manpower would not allow for the further setup of such instruments. However, the Nd:YAG laser that is the key component of the six-wavelength lidar is found in many other lidar systems around the world. With this laser it is comparably easy to generate laser light at three wavelengths, i.e., 355, 532, and 1064 nm, from which backscatter coefficients at these wavelengths and extinction coefficients at the UV and the visible wavelengths can be derived.<sup>13</sup>

Despite impressive results obtained with aerosol Raman lidars and newly developed inversion algo-

---

I. Veselovskii (irgorv@pic.troitsk.ru) and A. Kolgotin are with the Physics Instrumentation Center, Troitsk, Moscow Region 142190, Russia. D. Müller (detlef@tropos.de) is with the Institute for Tropospheric Research, Permoserstrasse 15, 04318 Leipzig, Germany. D. N. Whiteman (david.n.whiteman@nasa.gov) is with NASA Goddard Space Flight Center, Greenbelt, Maryland 20771.

Received 8 December 2004; revised manuscript received 17 March 2005; accepted 23 March 2005.

0003-6935/05/255292-12\$15.00/0

© 2005 Optical Society of America

rithms, many uncertainties still exist. In part these uncertainties are caused by the fact that in simulations mainly optical data, generated from synthetic particle size distributions, are used to investigate the possibilities of particle characterization. Simplifications in these simulations as well as the extreme time consumption that arises from these simulations still do not allow us to give a final answer to many questions laid out in the sensitivity analyses and to provide the aerosol lidar research community with a final picture of what can be expected from aerosol Raman lidar regarding microphysical particle characterization. Some of these questions are mentioned in the following.

In view of the simpler (from a technical point of view and also considering the costs of setting up sophisticated aerosol Raman lidars) three-wavelength aerosol lidar systems, extreme effort has been put on studies to answer the question, if a reduced data set of backscatter coefficients at three wavelengths and extinction coefficients at two wavelengths ( $3\beta + 2\alpha$ ) is equivalent to the set of backscatter coefficients at six wavelengths and extinction coefficients at two wavelengths ( $6\beta + 2\alpha$ ) regarding the accuracy of microphysical particle characterization. Results so far suggest that the use of data sets consisting of ( $3\beta + 2\alpha$ ) results in similarly accurate microphysical particle parameters, if measurement errors are low enough.<sup>8,14</sup> But at the same time one has to keep in mind that errors in any of the three backscatter coefficients of a three-wavelength lidar influence the quality of the derived parameters more than respective errors in any of the six backscatter coefficients of an upgraded aerosol lidar. Some doubt still remains about whether the increase in the number of particle backscatter coefficients and/or extinction coefficients could significantly improve the inversion results. What is the exact range for retrieving trustworthy parameters of atmospheric particle size distributions, i.e., effective radius, and the complex refractive index? Questions remain open concerning the simultaneous retrieval of the complex refractive index and the effective radius with little or no *a priori* information.

As mentioned above, one way of assessing the performance is through extensive numerical simulations for numerous particle size distributions and refractive indices. One has to keep in mind that the simulations are carried out for a specific set of measurement wavelengths and optical data. Furthermore these simulations basically have to be carried out anew, if the set of measurement wavelengths and the kind of data used are changed. So simulations become rather tedious, and at one point modeling becomes almost unmanageable.

An alternative approach, or rather a complementary approach, is given by analyzing the information content of lidar data with the help of the eigenvalue analysis.<sup>2,15</sup> This approach goes beyond the first publications in the field of aerosol research with lidar carried out in the past,<sup>16,17</sup> where the authors focused on using the eigenvalue analysis for the inversion process itself, rather than using it for exploration of

the limits and capabilities of a specific code. The eigenvalue analysis, as presented in this paper, is also a more fundamental analysis tool than techniques that attempt to identify the information content of the spectra of backscatter and/or extinction coefficients by testing, in simplifying words, the degree of difference in the optical data points at different wavelengths. For that purpose the optical data are calculated for the given shape of the particle-size distribution and given complex refractive indices.<sup>18</sup>

The advantage of the eigenvalue analysis is that it allows one to draw some rather general conclusions on the theoretically achievable accuracy of retrieved particle parameters, to test the effect of combining backscatter and extinction data in a rather straightforward manner, and to investigate the influence of kernel functions in different representations (volume, surface area, or number),<sup>9</sup> all this rather independently from the actual inversion algorithm used in the data analysis.

In this study we still kept certain limitations such as investigation of lognormal particle size distributions, as well as the use of a wavelength- and size-independent complex refractive index of the investigated particles. Investigations in which these constraints are less are beyond the scope of this paper but will be considered in future studies. After Section 1, we outline the mathematical concepts in Section 2. In Sections 3–5 we present results on simulations. In Section 6 we close with a summary and outlook.

## 2. Methodology

The particle backscatter  $\beta$  and extinction  $\alpha$  coefficients obtained from lidar data are related to aerosol size distributions  $f(r)$  as

$$\beta(\lambda) = \int_{r_{\min}}^{r_{\max}} f(r)K_{\beta}(r, m, \lambda)dr,$$

$$\alpha(\lambda) = \int_{r_{\min}}^{r_{\max}} f(r)K_{\alpha}(r, m, \lambda)dr.$$

The particle radius is  $r$ , the complex refractive index is  $m$ , and  $\lambda$  is the measurement wavelength. Terms  $K_{\beta, \alpha}$  are kernel functions and can be calculated on the basis of the Mie-scattering theory,<sup>19</sup> i.e., for spherical particles. The essence of the multiwavelength lidar technique is measurement of the spectrum  $\beta(\lambda)$  and  $\alpha(\lambda)$ . Changes in the particles' parameters, such as the particle-size distribution (PSD) or  $m$ , lead to variations in  $\beta(\lambda)$  and  $\alpha(\lambda)$ . If this spectrum is unique, i.e., function  $\beta_i(\lambda)$  or  $\alpha_i(\lambda)$  corresponding to different aerosol parameters are linearly independent, identification of these parameters becomes possible.

The spectral variations of the backscatter and the extinction coefficients for different aerosol sizes and refractive indices are exemplified in Figs. 1 and 2. Calculations are performed for lognormal size distributions,

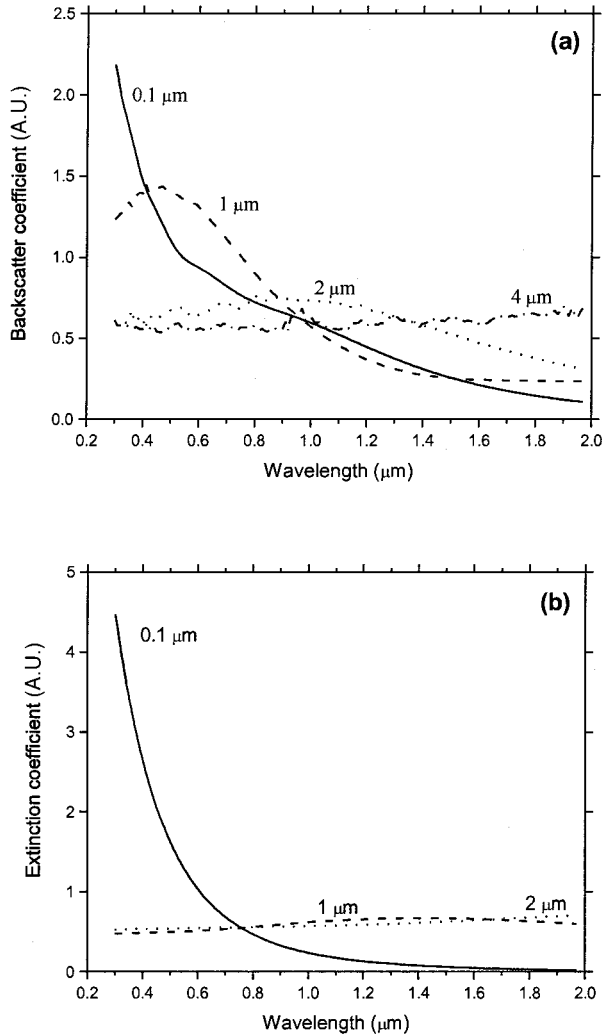


Fig. 1. Wavelength dependence of (a) backscattering and (b) extinction coefficients calculated for lognormal size distributions of spherical particles with  $r_0 = 0.1, 1, 2,$  and  $4 \mu\text{m}$ ;  $\ln \sigma = 0.4$ ,  $m = 1.33 - i0$ . All  $\alpha$  and  $\beta$  are normalized to  $\int \beta(\lambda) d\lambda = \int \alpha(\lambda) d\lambda = 1$  in the interval considered.

$$\frac{\partial n(r)}{\partial \ln r} = \frac{n_t}{(2\pi)^{1/2} \ln \sigma} \exp\left[-\frac{(\ln r - \ln r_0)^2}{2(\ln \sigma)^2}\right],$$

with a mode radius of  $0.1 \leq r_0 \leq 4 \mu\text{m}$  and a mode width of  $\ln \sigma = 0.4$  in the spectral wavelength range of  $0.3\text{--}2 \mu\text{m}$ . Here  $n_t$  denotes the total particle number. Such size distributions have effective radii, i.e., surface-weighted mean radii of  $0.15 < r_{\text{eff}} < 6 \mu\text{m}$ . For convenience of comparison the coefficients are normalized so that

$$\int \beta(\lambda) d\lambda = 1, \quad \int \alpha(\lambda) d\lambda = 1$$

for the chosen interval. For fixed  $m$  the functions  $\beta_i(\lambda)$  corresponding to  $r_0 = 0.1, 1,$  and  $2 \mu\text{m}$  are linearly independent. For  $r_0 = 2$  and  $4 \mu\text{m}$ , the functions  $\beta_i(\lambda)$ , however, become quite similar in the interval from

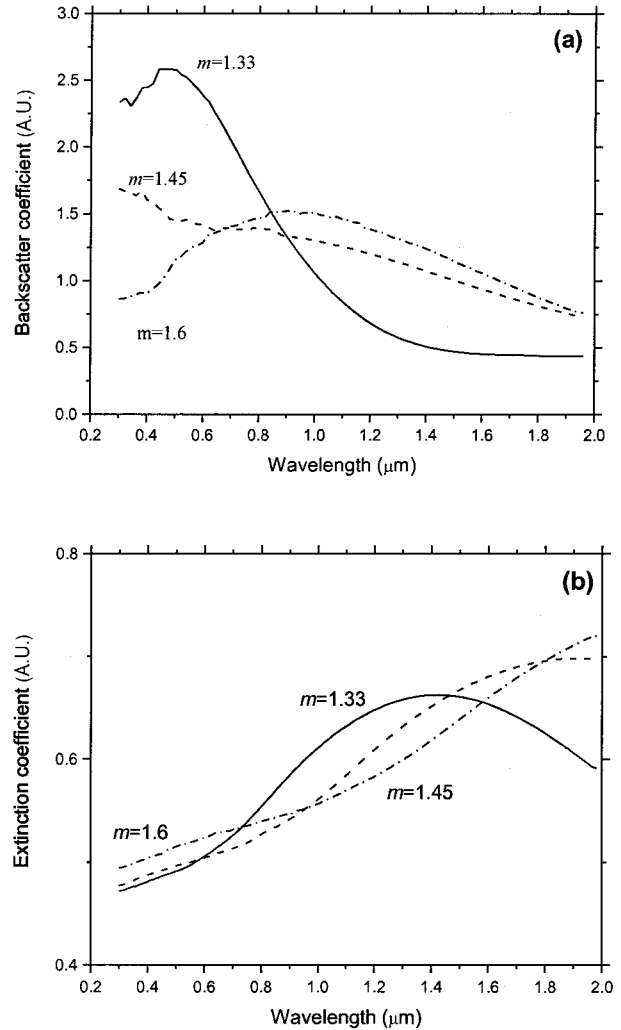


Fig. 2. Wavelength dependence of (a) backscatter and (b) extinction coefficients for refractive indices:  $m = 1.33 - i0, 1.45 - i0,$  and  $1.6 - i0$  calculated for a lognormal size distribution of spherical particles with  $r_0 = 1 \mu\text{m}$  and  $\ln \sigma = 0.4$ .

$0.35$  to  $1.06 \mu\text{m}$  (the range usually available in the lidar measurements), and the possibility of their separation depends on measurement accuracy. The variations in  $\beta_i(\lambda)$  for different refractive indices at  $r_0 = 1 \mu\text{m}$  are illustrated in Fig. 2. The functions  $\beta_i(\lambda)$  corresponding to  $m = 1.3, 1.45,$  and  $1.6$  are linearly independent, which provides the basis for retrieval of the refractive index.

Extinction coefficients are much more variable at fixed  $m$  for smaller particles compared with the respective backscatter coefficients. So  $\alpha$ , on the one hand, should be better suited for sensing the fine mode of the PSD. But, on the other hand, it must be kept in mind that extinction coefficients are not very sensitive to variations in the refractive index, as illustrated in Fig. 2(b), where variations in the dependence of the real part are shown. An even greater challenge is to estimate the imaginary part  $m_I$  of  $m$ . Figure 3 shows the spectral dependence of  $\beta_i(\lambda)$  and  $\alpha_i(\lambda)$  for fixed  $m_R = 1.45$  and  $m_I = 0, 0.01, 0.02$ .

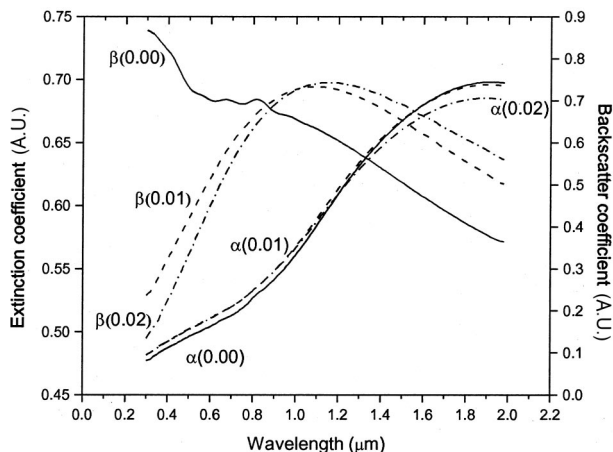


Fig. 3. Extinction and backscatter coefficients as a function of wavelength for a lognormal size distribution with  $r_0 = 1 \mu\text{m}$  and  $\ln \sigma = 0.4$  calculated at, solid curve,  $m_I = 0$ ; dashed curve, 0.01; dash-dot curve, 0.02;  $m_R = 1.45$ .

Calculations were performed for a lognormal size distribution with  $r_0 = 1 \mu\text{m}$  and  $\ln \sigma = 0.4$ . The backscatter coefficients for  $m_I = 0$  and  $m_I = 0.01$  are quite different; thus the different  $m_I$  can in principle be distinguished in the inversion. In contrast the  $\beta_i(\lambda)$  functions are much more similar for  $m_I = 0.01$  and  $m_I = 0.02$ , which makes retrieval of the imaginary part more difficult for large  $m_I$ . The extinction coefficients again show no sensitivity to the change in  $m_I$ . So the use of  $\alpha$  alone cannot supply information about the refractive index. In fact in previous simulations it was pointed out that the combined use of particle backscatter and extinction coefficients provides an optimum tool for identifying the mean particle size as well as the complex refractive index.

The complicated dependencies of the parameters presented in Figs. 1–3 have already pointed to difficulties in drawing a general conclusion on the possibility and accuracy of retrieving different particle parameters, and it is rather obvious that we need a rigorous quantitative criterion that, on the one hand, measures the linear independence of the functions presented in Figs. 1–3 and, on the other hand, can be related to the effect of measurement errors on the retrieval accuracy.

The linear independence of functions  $\beta_i(\lambda)$  obtained for different values of mode radius, mode width, and complex refractive index can be tested by minimizing the sum

$$\sum_i a_i \beta_i.$$

If this sum is zero for some set of  $a_i$ , i.e.,

$$\sum_i a_i^2 = 1,$$

the corresponding  $\beta_i(\lambda)$  are linearly dependent. The quadratic form

$$q = \int_{\lambda_{\min}}^{\lambda_{\max}} \left[ \sum_i a_i \beta_i(\lambda) \right]^2 d\lambda \quad (1)$$

can be taken as a quantitative measure of linear independence. Representing coefficients  $a_i$  and functions  $\beta_i$  in vector form,

$$\begin{bmatrix} a_1 \\ \dots \\ a_n \end{bmatrix} = \mathbf{a}, \quad \begin{bmatrix} \beta_1 \\ \dots \\ \beta_n \end{bmatrix} = \mathbf{B}, \quad (2)$$

we may rewrite Eq. (1) as

$$q = \int \mathbf{a}^* \mathbf{B} \mathbf{B}^* \mathbf{a} d\lambda = \mathbf{a}^* \mathbf{C}^\beta \mathbf{a}, \quad (3)$$

where  $\mathbf{C}^\beta$  is a matrix,  $c_{i,j} = \|\int \beta_i(\lambda) \beta_j(\lambda) d\lambda\|$ , and the asterisk is used to represent the transposition.

Vector  $\mathbf{a}$  may be decomposed as  $\mathbf{a} = \mathbf{U} \boldsymbol{\xi}$ , where  $\mathbf{U}$  is the matrix contained in its column eigenvectors of matrix  $\mathbf{C}^\beta$ :

$$q = \mathbf{a}^* \mathbf{C}^\beta \mathbf{a} = \boldsymbol{\xi}^* \mathbf{U}^* \mathbf{C}^\beta \mathbf{U} \boldsymbol{\xi}. \quad (4)$$

But  $\mathbf{U}^* \mathbf{C}^\beta \mathbf{U} = \boldsymbol{\Lambda}$ , where  $\boldsymbol{\Lambda}$  is a diagonal matrix consisting of eigenvalues  $l_i$  so that

$$q = \boldsymbol{\xi}^* \boldsymbol{\Lambda} \boldsymbol{\xi} = \sum_i l_i^\beta \xi_i^2. \quad (5)$$

The minimum of the quadratic form, Eq. (5), is determined by the smallest eigenvalue  $q_{\min} = l_{\min}^\beta$  of the covariance matrix  $\mathbf{C}^\beta$ . A detailed description of the concept of the eigenvalue analysis, as outlined here, can be found in Ref. 2. The set of coefficients  $a_i$ , which minimizes  $q$ , is determined by the corresponding eigenvector  $\mathbf{u}_{\min}$  of matrix  $\mathbf{C}^\beta$ .

If the  $\beta_i(\lambda)$  functions are measured with error  $\delta$ , condition  $l_{\min}^\beta > \delta^2$  has to be fulfilled in order to obtain the linear independence of  $\beta_i(\lambda)$ .<sup>2</sup> The same holds if extinction is considered. We keep in mind that  $\alpha(\lambda)$  and  $\beta(\lambda)$  are two independent parameters; thus the criterion of independence has to be fulfilled at least for one of these parameters. Moreover the combination of  $\alpha_i(\lambda)$  and  $\beta_i(\lambda)$  allows the retrieval even for the case in which each of these sets is linearly dependent. This may be understood from Fig. 4, which shows the wavelength dependence of the backscatter and extinction coefficients calculated for a lognormal size distribution with a mode radius of  $r_0 = 0.1 \mu\text{m}$  and a mode width of  $\ln \sigma = 0.4$ . The backscatter coefficients for  $m_r = 1.3$  and 1.5 show a similar spectral dependence; thus these curves are not independent. The same is true for extinction. This means that, using some scaling coefficient  $a$ , we can make  $\beta_i(\lambda)$  corresponding to  $m_r = 1.3$  and 1.5 coincide. But backscatter and extinction coefficients are two independent kinds of data. Hence we fail to resolve, e.g., the mean

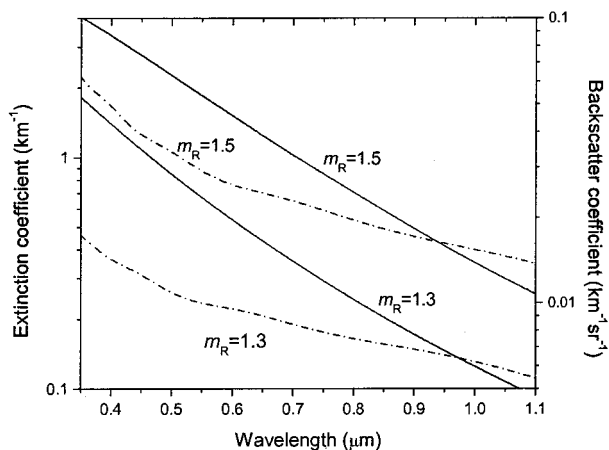


Fig. 4. Wavelength dependence of the, solid curves, extinction, and, dash-dot curves, backscatter coefficients for  $m = 1.3 - i0$  and  $m = 1.5 - i0$ . Calculations are performed for a lognormal size distribution with mode width  $\ln \sigma = 0.4$  and mode radius  $r_0 = 0.1 \mu\text{m}$ .

(effective) size of the particles, if their extinction coefficients  $\alpha_i(\lambda)$  also coincide for the same scaling coefficient  $a$ . In that case the particles have the same particle extinction-to-backscatter (lidar) ratio. Figure 5 shows, however, that the corresponding lidar ratios are different; so it can be assumed that a successful retrieval is still possible if  $\alpha_i(\lambda)$  and  $\beta_i(\lambda)$  are used simultaneously. Mathematically this means that for the combined use of  $\alpha_i(\lambda)$  and  $\beta_i(\lambda)$  we have to minimize the sum

$$q = \int_{\lambda_{\min}}^{\lambda_{\max}} \left[ \sum_i a_i \beta_i(\lambda) \right]^2 d\lambda + \int_{\lambda_{\min}}^{\lambda_{\max}} \left[ \sum_i a_i \alpha_i(\lambda) \right]^2 d\lambda. \quad (6)$$

It can be shown that the minimum of the quadratic form  $q_{\min} = l_{\min}^{\alpha+\beta}$  corresponds to the minimum eigenvalue  $l_{\min}^{\alpha+\beta}$  of the matrix  $(C^\beta + C^\alpha)$ .

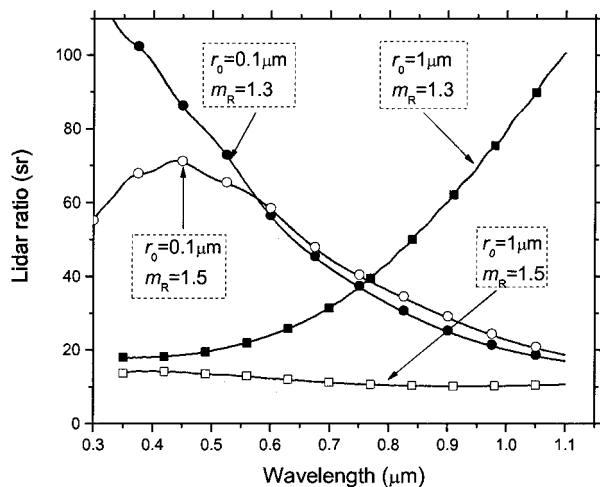


Fig. 5. Lidar ratio for, solid symbols,  $m = 1.3 - i0$  and, open symbols,  $m = 1.5 - i0$  calculated for mode radius, circles,  $r_0 = 0.1 \mu\text{m}$  and, squares,  $1 \mu\text{m}$ .

### 3. Numerical Test for the Linear Independence of Optical Data

The linear independence was tested for a set of  $\beta_i(\lambda)$ , which corresponds to different values of  $m(m_R, m_I)$  and mode radii  $r_0$ . As a first step we assume a lognormal aerosol size distribution, and the complex refractive index is kept size and wavelength independent. If we do not consider a mixture of particles with different  $m$ , the set  $\beta_{ij} = \beta(\lambda, m_i, r_{0j})$  is tested for the linear independence of each pair of elements: The first element  $\beta_{11}$  is compared with every element from the rest of the set; then this procedure is repeated for the second, third, and every following element. For  $M$  values of  $m_i$  and  $N$  values of  $r_{0j}$  the number of such pairs is

$$\sum_{i=1}^{M \times N - 1} (M \times N - i).$$

The dispersion of the lognormal distribution  $\ln \sigma$  at this stage is assumed to be constant, but in general the variation in the dispersion may be included also in the modeling. For each pair we form the covariance matrix, which is  $2 \times 2$  in size, and determine the corresponding eigenvalue  $l_{\min}^\beta$ . If the smallest  $l_{\min}$  for all pairs fulfills the requirement  $l_{\min}^\beta > \delta^2$ , the  $\beta_{ij}$  of the respective data set are linearly independent. The same analysis is performed for  $\alpha_{ij}$  and for the case of the combined use of extinction and backscatter coefficients. In that case the eigenvalues of the sum matrix are calculated, and the constraint  $l_{\min}^{\beta+\alpha} > \delta^2$  is tested.

For a comparison of eigenvalues with relative error in measurements, the correct normalization of the elements is essential. When we compare the element  $\beta_{ij}(\lambda)$  with the other elements in the set, we divide every element by the value

$$\sqrt{\int_{\lambda_{\min}}^{\lambda_{\max}} \beta_{ij}^2(\lambda) d\lambda},$$

so that the first element of the covariance matrix is always  $c_{1,1}^\beta = 1$ .

The same procedure is used for extinction. For the combined use of  $\beta_i(\lambda)$  and  $\alpha_i(\lambda)$  the minimal eigenvalue  $l^{\beta+\alpha}$  is divided by a factor of 2.

#### A. Estimating the Real and the Imaginary Parts of the Refractive Index for a Known Mode Radius

Before considering the general case, when  $m_R, m_I$ , and the mean radius are varied simultaneously, let us simulate several special cases that bring some insight into the contribution of each of these parameters. It will also put limits on the range where retrieval is possible. First, we consider the situation in which the modal radius of the particle is fixed while either  $m_R$  or  $m_I$  may be varied. The result is illustrated in Fig. 6 where the minimum eigenvalues are found for the chosen mode radii  $r_0$ . Calculations

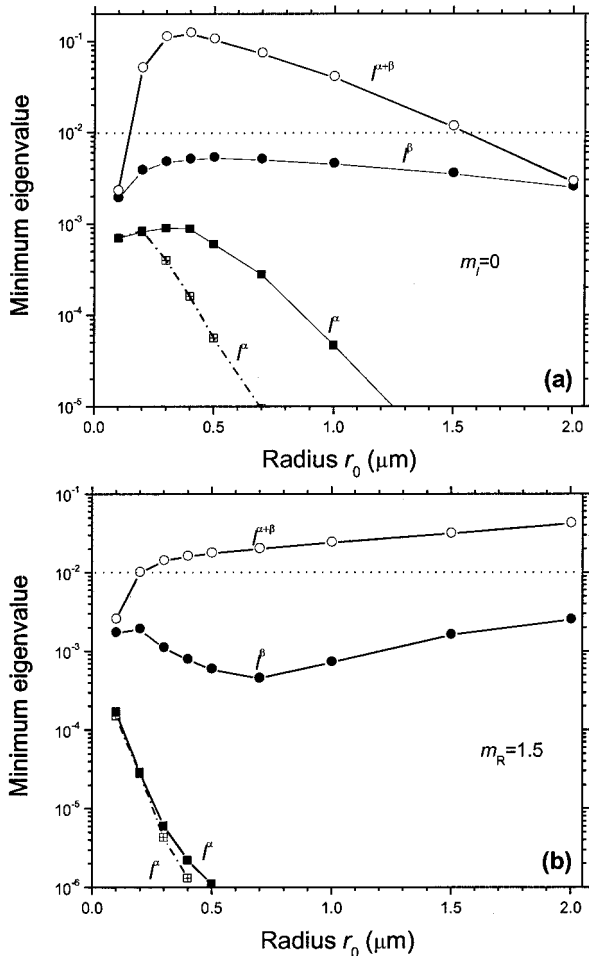


Fig. 6. Minimal eigenvalues calculated from squares,  $\alpha(\lambda)$ ; solid circles,  $\beta(\lambda)$ ; and, open circles, their combination for different fixed values of mean radius  $r_0$ . (a) The real part of the refractive index was varied from  $m_R = 1.3$  to  $m_R = 1.6$  with a step width of  $\Delta m_R = 0.1$ , while  $m_I$  was kept fixed at  $m_I = 0$ . (b) The imaginary part was varied from  $m_I = 0$  to  $0.02$  with a step width of  $0.01$ , while  $m_R$  was kept fixed at  $m_R = 1.5$ . The values for  $\beta(\lambda)$  and  $\alpha(\lambda)$  cover the wavelength range from  $0.35$  to  $1.06 \mu\text{m}$ , except for the dash-dot curve (squares with crosses) that shows the case for  $\alpha(\lambda)$  in the interval from  $0.35$  to  $0.53 \mu\text{m}$ .

lations are performed for a lognormal size distribution with  $\ln \sigma = 0.4$ . The results are smoothed to remove small-scale variations that are irrelevant in our analysis. The values for  $\beta_i(\lambda)$  and  $\alpha_i(\lambda)$  cover the wavelength range of  $0.35$ – $1.06 \mu\text{m}$ , except for the dash-dot curve that shows in addition the case for  $\alpha_i(\lambda)$  in the  $0.35$ – $0.53 \mu\text{m}$  interval. The horizontal dotted line indicates the level corresponding to a 10% measurement error. As we can see the use of only backscattering  $l^\beta$  or extinction  $l^\alpha$  does not allow us to retrieve the refractive index, because these values are linearly dependent. But their combined use  $l^{\beta+\alpha}$  allows us to perform successful retrievals of  $m_R$  in the  $0.15 < r_0 < 1.5 \mu\text{m}$  ( $0.225 < r_{\text{eff}} < 2.25 \mu\text{m}$ ) size range.

In practical application particle extinction is available only in the wavelength range from  $0.35$  to

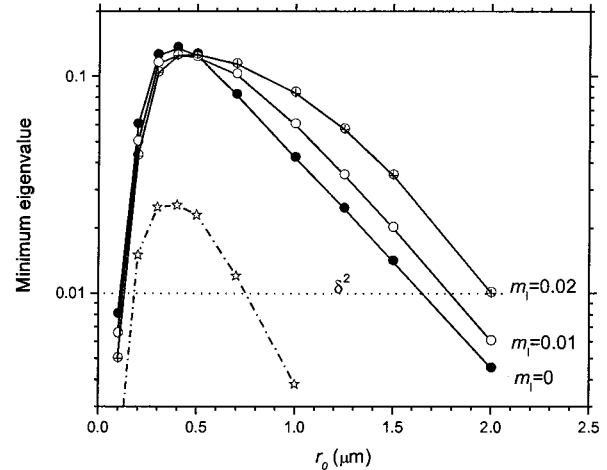


Fig. 7. Minimum eigenvalues for different fixed values of mean radius  $r_0$  calculated from a combination of  $\alpha(\lambda)$  and  $\beta(\lambda)$  for  $m_I = 0, 0.01, 0.02$ . The real part of the refractive index varied from  $1.3$  to  $1.6$  with a step width of  $0.1$ ; dash-dot curve (open stars), results for  $m_I = 0$  and  $\Delta m_R = 0.05$ ; horizontal dotted line, level corresponding to a measurement error,  $\delta = 10\%$ .

$0.53 \mu\text{m}$ , which would be a critical constraint if only extinction information were used for data inversion. But if extinction and backscatter coefficients are used together, the result practically does not depend on the chosen wavelength interval of  $\alpha(\lambda)$ . This result follows from Fig. 5: Even for  $r_0 = 1 \mu\text{m}$  the lidar ratios for the chosen values of the complex refractive index are different at short wavelengths. Comparing Figs. 6(a) and 6(b), we see that for the chosen parameters variations in the real part of the refractive index may not be resolved by inversion schemes for large particle radii ( $r_0 > 1.5 \mu\text{m}$ ), whereas variations in the imaginary part may not be resolved at small particle radii ( $r_0 < 0.2 \mu\text{m}$ ,  $r_{\text{eff}} < 0.3 \mu\text{m}$ ).

To illustrate the influence of the imaginary part  $m_I$ , Fig. 7 shows the minimum eigenvalues calculated for the same parameters as in Fig. 6(a), but for  $m_I = 0, 0.01, 0.02$ . The real part of the refractive index is varied from  $1.3$  to  $1.6$  with a step width of  $0.1$ . Calculations were performed for the  $\alpha_i(\lambda)$  and  $\beta_i(\lambda)$  combination, since it is clear from Fig. 6 that the separate use of these data does not allow us to perform the retrieval. The minimum eigenvalue for big  $m_I$  is increased; thus for fixed (known)  $r_0$  and  $m_I$  the increase in  $m_I$  does not decrease the accuracy of the inversion. The plot also shows the result for  $\Delta m_R = 0.05$  and  $m_I = 0$ . In this case the minimum eigenvalue is dramatically decreased. Hence even for fixed  $r_0$  and  $m_I$  a realistic estimation of the real part of the refractive index is not better than  $\pm 0.05$ , and the variation in the mean radius will only degrade the accuracy. We point out that the uncertainty in  $\pm 0.05$  is in reasonable agreement with the results from our previous simulation studies.<sup>8,9</sup>

In the next step we consider how much the range in  $m_I$  variation for the chosen  $m_R$  and  $r_0$  influences the interdependence of the spectra. Figure 8 shows the minimum eigenvalues for different fixed values of the

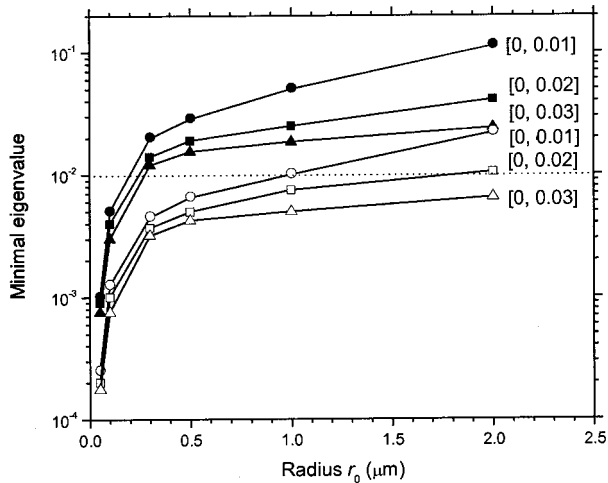


Fig. 8. Minimal eigenvalues for different fixed values of mean radius  $r_0$  calculated from the combination of  $\alpha_i(\lambda)$  and  $\beta_i(\lambda)$ . The real part of the refractive index was kept fixed at  $m_R = 1.5$ , while the imaginary part was varied at intervals: circles, [0, 0.01]; squares, [0, 0.02]; triangles, [0, 0.03] with a step width of, solid symbols, 0.01; open symbols, 0.005.

radius  $r_0$ , when the imaginary part  $m_I$  is varied in the intervals of 0–0.01, 0–0.02, and 0–0.03. The calculations are performed for two values of step width, i.e.,  $\Delta m_I = 0.01$  and 0.005. The real part was set at  $m_R = 1.5$ . Figure 3 shows that the backscatter coefficient changes strongly when  $m_I$  varies from 0 to 0.01, but a further increase in the imaginary part does not produce such pronounced changes. This result agrees with the results in Fig. 8 where the eigenvalues decrease with the increase in the interval of variation of  $m_I$ . The minimum eigenvalues depend on the step width  $\Delta m_I$  used in the calculations, thus defining the possible accuracy of the retrieval of  $m_I$ . For example, for a 10% measurement error, the imaginary part can be estimated with an accuracy of  $\pm 0.005$ . It is obvious that introducing the variations of  $r_0$  and  $m_R$  only increases the corresponding uncertainty.

In the following step  $m_R$  and  $m_I$  are varied simultaneously for the chosen  $r_0$ . Such a situation is illustrated in Fig. 9, where again the minimum eigenvalues are calculated from a combination of  $\alpha_i(\lambda)$  and  $\beta_i(\lambda)$ . For  $m_I$  varying in the interval from 0 to 0.01 the minimum eigenvalues are determined mainly by variations of  $m_I$  for  $r_0 < 0.5 \mu\text{m}$  and by variations of  $m_R$  for  $r_0 > 1 \mu\text{m}$ . Thus the retrieval of  $m$  can be done in the  $0.2 \mu\text{m} < r_0 < 1.4 \mu\text{m}$  interval. If  $m_I$  is varied in the interval from 0 to 0.03, the eigenvalues are much lower than those obtained when either  $m_R$  or  $m_I$  are fixed and the retrieval of the refractive index becomes impossible for any radius. So, if we have no preliminary information about the imaginary part, the retrieval of the refractive index even in the case of an *a priori* known radius is possible only for low absorbing particles with  $m_I \sim 0.02$ .

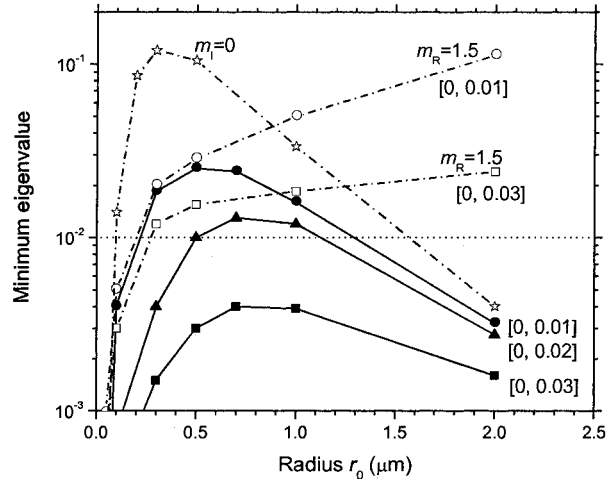


Fig. 9. Minimum eigenvalues for different fixed values of mean radius  $r_0$  calculated from the combination of  $\alpha_i(\lambda)$  and  $\beta_i(\lambda)$ . The real part of the refractive index  $m_R$  is varied from 1.3 to 1.6 with  $\Delta m_R = 0.1$ , while  $m_I$  is varied in the intervals: circles, [0, 0.01]; triangles, [0, 0.02]; squares, [0, 0.03] with a step width of  $\Delta m_I = 0.01$ . Also shown for comparison are the results for fixed  $m_I = 0$ , while  $m_R$  is varied, open stars, and for a fixed  $m_R = 1.5$  when  $m_I$  is varied in the interval, open circles, [0, 0.01]; open squares, [0, 0.03].

#### B. Estimating the Mean Radius for the Known Refractive Index

In the following analysis we consider the possibility of estimating the aerosol mean radius. In the beginning it is assumed that  $m_R$  and  $m_I$  are known. Figure 10 illustrates the retrieval of the particles mean radius for fixed values of  $m$ . Eigenvalues are calculated at the interval  $[r_{0 \min}, r_{0 \max}]$  with  $r_{0 \min} = 0.05 \mu\text{m}$  in all computations. For every value of  $r_{0 \max}$  eigenvalues

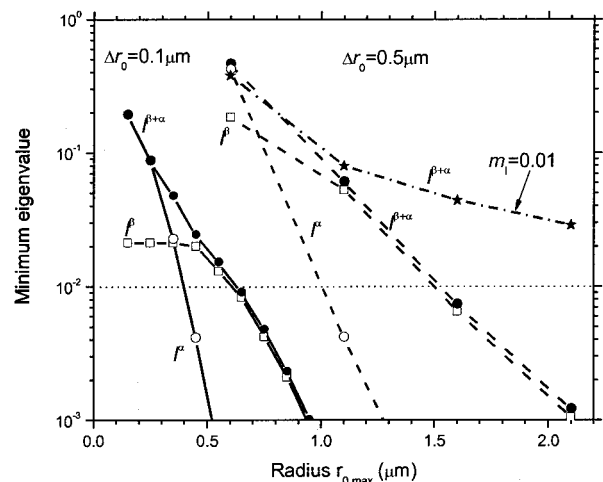


Fig. 10. Minimum eigenvalue as a function of  $r_{0 \max}$  calculated from, open squares,  $\beta_i(\lambda)$ ; open circles,  $\alpha_i(\lambda)$ ; and, solid circles, their combination. The calculations are performed in the radius interval  $[r_{0 \min}, r_{0 \max}]$ ,  $r_{0 \min} = 0.05 \mu\text{m}$ ;  $r_{0 \max}$  is varied by a step width of 0.1 and  $0.5 \mu\text{m}$ . The complex refractive index is  $m = 1.5 - i0$ ; solid stars, result obtained for a combination of  $\beta_i(\lambda)$  and  $\alpha_i(\lambda)$  for  $m = 1.5 - i0.01$ .

are calculated by comparing the corresponding element with all other elements of the set, as described in Section 2. The minimum of these eigenvalues  $l_{\min}$  is plotted in Fig. 10.

It is known that for a given refractive index  $m$  the kernel functions corresponding to  $\alpha$  are more suitable for the retrieval of small radii compared with the corresponding kernel functions for  $\beta$ .<sup>9,17</sup> For fixed, i.e., known  $m$  the coefficients  $\alpha_i$  or  $\beta_i$  are linearly independent (as shown in Fig. 1) so their combination does not lead to a pronounced effect. The minimum eigenvalue depends on the step width of the variation of  $r_0$ . The larger that  $\Delta r_0$  is the more independent are the elements; thus this value is a measure of the possible radius resolution in lidar measurements. For a lognormal size distribution with  $\ln \sigma = 0.4$  it is possible to retrieve particle sizes as large as  $r_0 = 0.6 \mu\text{m}$  ( $r_{\text{eff}} = 0.9 \mu\text{m}$ ) on the basis of a resolution of  $\Delta r_0 = 0.1 \mu\text{m}$ . In contrast the retrieval of a particle size with  $r_0 = 1.5 \mu\text{m}$  is possible with a resolution of only  $0.5 \mu\text{m}$ . For illustration Fig. 10 also shows the results for absorbing particles with  $m_I = 0.01$ . The absorption introduces an additional dependence of the scattering parameters on the particle radius. Consequently the retrieval of the PSD becomes possible for significantly larger radii if the refractive index is known. This result has already been found from the simulation studies in Ref. 9.

### C. Estimating the Mean Radius for the Unknown Real or the Imaginary Part of the Refractive Index

If the variations of  $m_R$  or  $m_I$  are added to the variations of  $r_0$ , the radius interval for which the retrieval is possible decreases. This effect is illustrated in Fig. 11, which shows the minimum eigenvalues calculated from the combination of  $\alpha_i(\lambda)$  and  $\beta_i(\lambda)$ , if the radius is varied in the interval from  $0.05 \mu\text{m}$  to  $r_{0 \text{ max}}$ . In principle the variation of  $r_0$  may be performed with a constant step width, as was done in Fig. 10, but the situation in which the step width is taken as a fraction of  $r_0$  is more representative. For the curve in Fig. 11 every value of  $r_0$  is obtained by doubling the previous one. The comparison is performed for elements corresponding to  $r_0$  and  $r_0/2$ . Thus the step width is  $\Delta r_0 = r_0/2$ , and the corresponding accuracy is 50%.

Two situations are considered. First, the real part of the refractive index  $m_R$  is varied from 1.3 to 1.6 with  $\Delta m_R = 0.1$ , whereas the imaginary part is  $m_I = 0$  (solid circles). Second,  $m_R$  is fixed ( $m_R = 1.5$ ), whereas  $m_I$  is varied from 0.0 to 0.03 with a step width of  $\Delta m_I = 0.01$  (open circles). In the first case the variations of  $m_R$  for the chosen  $\Delta m_R$ ,  $\Delta r_0$ , and  $\delta = 10\%$  allows retrieval in the  $0.15\text{--}1.3 \mu\text{m}$  interval. In the second case for  $r_{0 \text{ min}} < 1 \mu\text{m}$  the minimum eigenvalue is determined mainly by the variations of  $m_I$  at fixed  $r_0$ , and the retrieval with a given resolution is possible only for mode radii exceeding  $\sim 0.2 \mu\text{m}$ . The dash-dot lines show the results when two parameters are fixed:  $m_R$  and  $m_I$  (open squares),  $m_I$  and  $r_0$  (solid stars),  $m_R$  and  $r_0$  (open stars). These

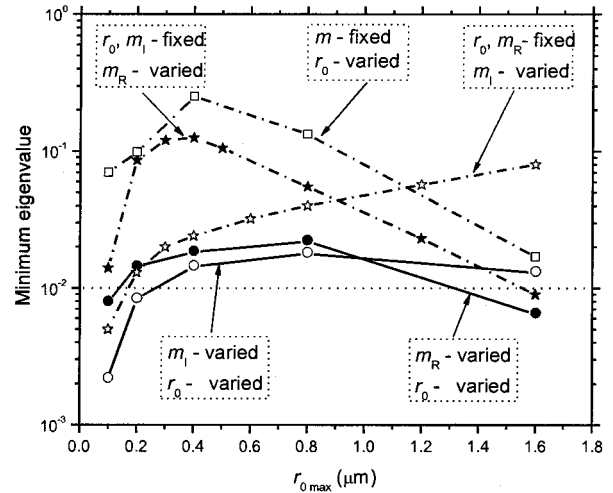


Fig. 11. Minimum eigenvalues calculated from the combination of  $\alpha_i(\lambda)$  and  $\beta_i(\lambda)$  when two parameters are varied: solid circles,  $r_0$  and  $m_R$ ; open circles,  $r_0$  and  $m_I$ . The real part of the refractive index  $m_R$  is varied from 1.3 to 1.6 with  $\Delta m_R = 0.1$ , while, solid circles,  $m_I = 0$ . The imaginary part of the refractive index  $m_I$  is varied from 0.0 to 0.03 with  $\Delta m_I = 0.01$ , while, open circles,  $m_R = 1.5$ . The calculations are performed in a radius interval of  $[r_{0 \text{ min}}, r_{0 \text{ max}}]$ ,  $r_{0 \text{ min}} = 0.05 \mu\text{m}$ , and a step width of  $\Delta r_0 = r_0/2$ . For comparison the dash-dot curves show the results when two parameters are fixed: open squares,  $m_R$  and  $m_I$ ; solid stars,  $r_0$  and  $m_I$ ; open stars,  $r_0$  and  $m_R$ .

dash-dot lines limit the range of a successful retrieval. The simultaneous variation of the two parameters may only decrease the eigenvalues.

### D. Simultaneously Estimating the Mean Radius and Complex Refractive Index

In Subsection 3.C we considered the case of retrieving the mean size if either of the other two parameters (the real or the imaginary part) is unknown. Finally in this subsection we consider the situation in which no *a priori* information about  $r_0$ ,  $m_R$ ,  $m_I$  is available. When the mean radius and the refractive index are varied simultaneously the final result is determined by the value of either  $\Delta m$  or  $\Delta r_0$ ; we are interested in separating these two effects. For example, Fig. 11 shows that for particles with  $r_0 < 0.1 \mu\text{m}$  the variation of  $m_R$  does not allow the simultaneous retrieval of the radius and refractive index. So the question arises of whether the retrieval of  $r_0$  alone is possible. The same is true for the refractive index: We are looking for situations in which the retrieval of  $m$  alone is possible. In other words, we want to find the range of parameters where  $m$  and  $r_0$  variations are linked and the range where these variations may be separated.

The variations of the parameters may be illustrated by the following matrix:

$$\begin{pmatrix} (r_1, m_1) & (r_2, m_1) & \dots & (r_N, m_1) \\ (r_1, m_2) & (r_2, m_2) & \dots & (r_N, m_2) \\ \dots & \dots & \dots & \dots \\ (r_1, m_M) & (r_2, m_M) & \dots & (r_N, m_M) \end{pmatrix}$$

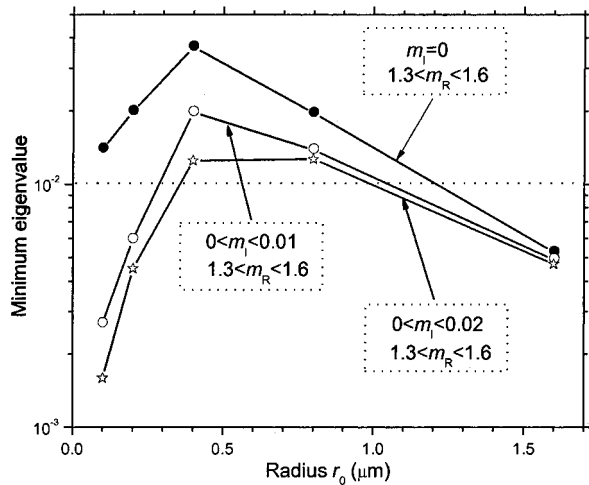


Fig. 12. Possible ways to estimate the complex refractive index. The minimum eigenvalue is shown as a function of radius. Comparisons between the elements with different radii but the same values of  $m$  are excluded. Calculations are performed, solid symbols, for fixed value  $m_I = 0$  and for  $m_I$  varied in the interval range of, open circles,  $[0; 0.01]$  and, open stars,  $[0; 0.02]$  with  $\Delta m_I = 0.01$  and  $\Delta m_R = 0.15$ . The eigenvalues are determined for the radius interval  $[r_{0 \min}, r_{0 \max}]$  with  $r_{0 \min} = 0.05 \mu\text{m}$  and a step width of  $\Delta r_0 = r_0/2$ .

If we exclude the comparison between the elements within the same column, we pursue only an estimation of the radius and neglect the possibility of the retrieval of the refractive index. On the contrary, if we exclude the comparison between the elements in the same row (elements having the same  $m$  but different radii), we consider only the possibility of retrieving the refractive index.

The retrieval of the refractive index is illustrated in Fig. 12. Considering the comments above, the comparison between the elements with different radii but the same values of  $m$  are excluded. Simulations were performed for the combination of  $\alpha_i(\lambda)$  and  $\beta_i(\lambda)$ . The step width of the radius variation was  $\Delta r_0 = r_0/2$ . The backscatter coefficient was considered for the wavelength interval from  $0.35$  to  $1.06 \mu\text{m}$ , whereas extinction was considered for the interval from  $0.35$  to  $0.53 \mu\text{m}$ . The step width was  $\Delta m_R = 0.15$ , which is equivalent to an accuracy of  $\pm 0.075$ . The step width of the imaginary part was  $\Delta m_I = 0.01$ . For transparent (nonabsorbing) aerosols ( $m_I = 0$ ) and 10% error in the lidar data the retrieval of the real part of the refractive index can be performed in the particle size range of  $0.1 \mu\text{m} < r_0 < 1.2 \mu\text{m}$ . In the middle of this interval the eigenvalues are approximately  $l_{\min} \sim 0.03$ ; thus for transparent aerosols,  $m_R$  may be retrieved even with higher accuracy, i.e.,  $\pm 0.05$ . The situation becomes more difficult when the range of variation of  $m_I$  rises. The size range for which the refractive index can be retrieved reduces to  $0.3 \mu\text{m} < r_0 < 1 \mu\text{m}$  if  $0 < m_I < 0.01$ . For  $0 < m_I < 0.02$  the range is decreased further and the eigenvalues become close to the threshold value of  $0.01$ , which means that we push our technique to the edge and

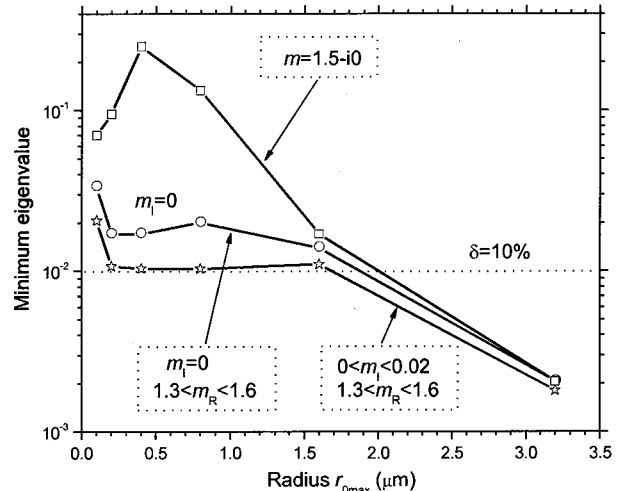


Fig. 13. Estimations of the particles' size when the refractive index is unknown. The minimum eigenvalue is shown as a function of  $r_{0 \max}$  for  $m_R$  varying in the range of  $1.3 < m_R < 1.6$  with  $\Delta m_R = 0.15$ ; circles,  $m_I$  varying in the range of  $0 < m_I < 0.02$  with  $\Delta m_I = 0.01$ . The plot also shows the results for transparent particles (circles,  $m_I = 0$ ) and for the case, when the refractive index of  $m = 1.5 - i0$  is assumed known. The eigenvalues are determined at a radius interval of  $[r_{0 \min}, r_{0 \max}]$ ,  $r_{0 \min} = 0.05 \mu\text{m}$ , and a step width of  $\Delta r_0 = r_0/2$ .

the retrieval procedure may become unstable. So any preliminary information about the expected range of  $m_I$  variations would improve the retrieval.

Figure 13 illustrates the possibility of estimating the mean radius. Retrievals were done for  $m_I = 0$  and  $0 < m_I < 0.02$ , while  $m_R$  was always varied in the range from  $1.3$  to  $1.6$ . For comparison we also show the results for the fixed value of  $m = 1.5 - i0$ . The influence of  $m_I$  on the retrieval of the mean radius is not as critical, which has been found from studies of simulations with inversion codes. For  $0 < m_I < 0.02$  the mode radius may still be retrieved in the range from  $0.1$  to  $1.7 \mu\text{m}$ . It is interesting that for  $r_0 < 0.2 \mu\text{m}$  the eigenvalues start to rise, approaching the value corresponding to the situation with fixed  $m$ . This fact has a simple interpretation. Figure 4 shows that for a fixed small value of  $r_0$  the spectra,  $\beta_i(\lambda)$  or  $\alpha_i(\lambda)$ , corresponding to different  $m_i$  are similar. But this means that for different radii  $r_{0i}$  these spectra differ (because for fixed  $m$  the spectra corresponding to different small  $r_0$  are independent, as shown in Fig. 10). Hence in this range the influence of  $m$  and  $r$  may be separated, and retrieval of the radius of the mean particle size is possible although the retrieval of  $m$  is not. On the contrary, in the size range of  $0.2 \mu\text{m} < r_0 < 1.5 \mu\text{m}$  the variations of  $m$  and  $r_0$  are coupled. This means that if  $m$  cannot be retrieved, we also fail to retrieve  $r_0$ .

#### 4. Number of Independent Pieces of Information in the Spectra of Backscatter and Extinction Coefficients

In our discussion we considered an infinite number of measurement wavelengths. For practical application it is important to know how many wave-

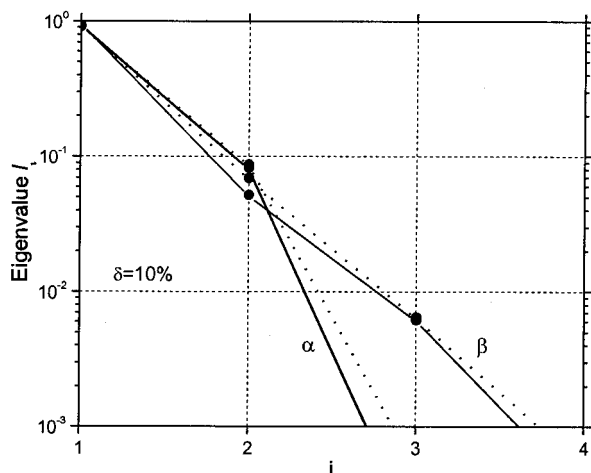


Fig. 14. First four eigenvalues of the covariance matrix calculated for backscatter and extinction coefficients: solid lines, refractive index kept fixed at  $m = 1.45 - i0$ ; dotted lines, case in which  $m_R$  and  $m_I$  are varied within the range of 1.3–1.6 and 0–0.02, respectively.

lengths are needed to properly represent the spectra of  $\beta(\lambda)$  or  $\alpha(\lambda)$ . This means that we have to investigate the degree of independence of the points of the curves  $\beta(\lambda)$ ,  $\alpha(\lambda)$ . Or, in other words, we have to determine how many independent pieces of information are contained in the variations of spectra  $\beta(\lambda)$  or  $\alpha(\lambda)$ , resulting from changes in PSD and refractive index. Such an analysis again rests on calculation of the eigenvalues  $l_i$  of the covariance matrix  $\mathbf{C}^\beta = \|\int \beta_i(\lambda)\beta_j(\lambda)d\lambda\|$ .

The set of spectra of backscatter  $\beta_i(\lambda)$  or extinction coefficients  $\alpha_i(\lambda)$  was generated for a wide range of mean radii  $r_0$  and refractive indices  $m$ :  $0.05 \mu\text{m} < r_0 < 1.5 \mu\text{m}$ ,  $1.3 < m_R < 1.6$ ,  $0 < m_I < 0.02$ . The simulations were carried out for lognormal distributions with mode width  $\ln \sigma = 0.4$ . The spectra were normalized so that  $\int \beta^2(\lambda)d\lambda = 1$ , and the elements of the covariance matrices were divided by the number of elements in the respective set in order to keep

$$\sum_i l_i = 1.$$

The number of characteristic patterns (independent pieces of information) is determined by the  $i$ th eigenvalue for which  $l_i < \delta^2$ . The  $i$ th eigenvalue contributes the corresponding characteristic pattern to the overall power

$$\sum_i \int \beta_i^2(\lambda)d\lambda.$$

Figure 14 illustrates the information content of the  $\beta(\lambda)$  and  $\alpha(\lambda)$  data. The eigenvalues  $l_i$  are plotted as a function of eigenvalue number  $i$ . The solid lines show the results if  $r_0$  is varied for a fixed  $m$ . The dotted lines correspond to the situation in which the varia-

tions of  $m$  are added. The third eigenvalue in the  $\beta(\lambda)$  variations is approximately  $6 \times 10^{-3}$ ; thus for a 10% measurement error ( $\delta^2 = 0.01$ ), variations in the backscatter coefficients contain no more than three independent pieces of information. Variations in the particle-extinction coefficient contain even a smaller number of characteristic patterns (approximately two). It must be kept in mind that such an analysis can provide only an estimate of the required number of wavelengths, but we can conclude that measuring  $\beta$  at three proper wavelengths and  $\alpha$  at two wavelengths may cover a significant part of the information contained in the spectrum of  $\beta(\lambda)$  and  $\alpha(\lambda)$ . It is interesting that the introduction of varying  $m$  does not significantly increase the number of characteristic patterns. This means that corresponding variations are not completely linearly independent, which agrees with the results in Fig. 13.

## 5. Information Content with Respect to the Variable Number of Backscatter Coefficients

In the following we briefly explore the effect of adding additional measurement wavelengths to the set of three backscatter and two extinction coefficients, which are available in practical applications. For that purpose we consider the measurement wavelengths at 400, 710, and 800 nm from which additional backscatter coefficients can be retrieved.<sup>12</sup> The effect of adding wavelengths may be revealed by analyzing the interdependence of kernel functions at the wavelengths of interest. The more distinct the kernels are, the higher their information content, and the solution is less sensitive to errors in measurements.

The objective method for analyzing the set of interdependence of the kernels may again be found in Ref. 2. The method is based on consideration of the covariance matrix

$$D = \left\| \int_{r_{\min}}^{r_{\max}} K_i(r)K_j(r)dr \right\|,$$

the elements of which are the projections of the kernels to one another;  $l_i$  are the corresponding eigenvalues of this matrix. The kernels may be considered independent if  $l_{\min} > \delta^2$  for the given mean error of the optical data.<sup>2</sup> The use of additional optical data inside the given wavelength interval can only decrease  $l_{\min}$ . Thus use of additional data is only of advantage if the minimum eigenvalue stays above a certain limit.

Extinction and in particular backscatter efficiencies are strongly oscillating,<sup>6,8</sup> so that the direct application of the analysis of the eigenvalues meets an obstacle; i.e., high-frequency oscillations of the kernels make them independent. However, real aerosol particles are distributed in size, and in inversion algorithms<sup>6,8</sup> the kernels are convoluted with base functions overextending ranges of particle radii. For these reasons these high-frequency oscillations are irrelevant in the following analysis.

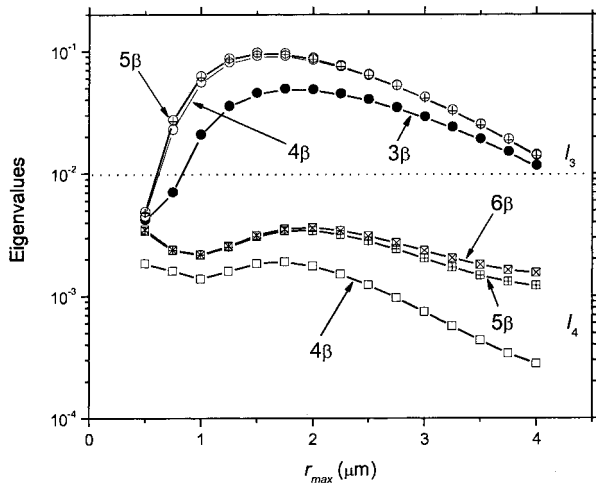


Fig. 15. Eigenvalues as a function of  $r_{0\max}$ : circles, third eigenvalue; squares, fourth eigenvalue. Calculations are performed at an interval of  $[r_{0\min}, r_{0\max}]$ ;  $r_{0\min} = r_{0\max}/5$  for three backscattering coefficients (solid circles,  $3\beta$ ) at 355, 532, and 1064 nm wavelengths. The plot also shows the eigenvalues for backscattering at 400 nm (open circles,  $4\beta$ ), 710 nm (circles with crosses,  $5\beta$ ) and 800 nm (squares with crosses,  $6\beta$ ) are added. The refractive index is  $1.45 - i0$ . The volume kernels are smoothed with a size distribution with  $\ln \sigma = 0.4$ : dotted line, level corresponding to 10% measurements errors.

In the present analysis high-frequency oscillations were smoothed by integrating kernels over the log-normal size distribution with  $\ln \sigma = 0.4$ . The smoothed kernels  $\tilde{K}_i(r_0, m)$  were used to calculate the elements of the covariance matrix  $\mathbf{D}$ . The kernels were normalized according to

$$\int_{r_{0\min}}^{r_{0\max}} \tilde{K}_i^2(r_0, m) dr_0 = 1,$$

where  $[r_{0\min}, r_{0\max}]$  is the interval at which the kernels' interdependence is tested.

We are interested in a study of the interdependence of the kernels at different radii intervals; thus the integration window  $[r_{0\min}, r_{0\max}]$  slides over the radius range. Figure 15 shows the third ( $l_3$ ) and fourth ( $l_4$ ) eigenvalue as a function of  $r_{0\max}$ , calculated for the interval  $[r_{0\min}, r_{0\max}]$  and  $r_{0\min} = r_{0\max}/5$ ; the refractive index was set to  $m = 1.45 - i0$ . Calculations were performed for three backscatter coefficients, i.e., at 355, 532, and 1064 nm wavelengths, that represent the kernel functions in terms of the particle number, e.g., Ref. 9.

The plot also shows the eigenvalues when backscatter coefficients at 400, 710, and 800 nm are added. The dotted line shows the level corresponding to 10% measurements errors. For three backscatter coefficients the kernel functions may be considered independent in a size range of  $0.75 \mu\text{m} < r_{0\max} < 4 \mu\text{m}$ . Increasing the number of backscatter coefficients leads to the appearance of higher-order eigenvalues that are lower than the noise level. Thus

there is no improvement in the radius resolution. At the same time the value for  $l_3$  rises, which means that the retrieval becomes more stable. To improve resolution in determining the mean size of the PSDs by the use of six backscatter coefficients, it is necessary to measure particle backscatter coefficients to an accuracy of at least 5%.

The analysis as outlined here in principle can also be used to analyze the importance of using different types of kernel functions, i.e., if the kernels are represented in terms of number, surface area, volume, or higher-order concentration. Such questions have been addressed in a previous paper<sup>9</sup> on the basis of simulations with synthetic data. A respective analysis goes beyond the present paper but will be considered in future studies.

## 6. Conclusion

For the first time, to our knowledge, a detailed study of the information content of multiwavelength lidar data based on the analysis of eigenvalues has been presented. Motivation for this approach is the fact that in recent years newly designed inversion algorithms have been routinely used for data analysis from lidar observations.<sup>6-10</sup> Unfortunately until now no mathematical framework has existed to explain in advance how accurately particle parameters can be derived for a given set of measurement wavelengths. Consequently it is almost impossible to generalize results from simulation studies. Changes in the measurement wavelengths used, in the number and kind of optical data (backscatter and extinction coefficients), or any other input parameter, as well as the connection of different parameters to one another during the inversion procedure, require additional sensitivity studies. The concept of eigenvalue analysis as used in the present studies is a first and certainly in some part a still rather simple step toward a more general mathematical framework to be developed in future work. Furthermore results from this eigenvalue analysis provide valuable insight into the reliability of the results that we obtained from past simulation studies.

In the following the main results from the study are summarized and compared with our results from previous simulation studies carried out with the inversion algorithm for synthetic data sets.

(1) The eigenvalue analysis confirmed the importance of combining particle backscatter and extinction coefficients. This importance has already been demonstrated in previous sensitivity studies.<sup>6,7,10</sup> It showed that extinction coefficients are a crucial input quantity and that situations where only backscatter coefficients may be sufficient are very limited. The importance of the analysis presented here is that it provides, first, hints of the underlying mechanism that leads to stabilization of the inverse problem.

(2) The present analysis demonstrates that the accuracy of an  $r$  and  $m$  estimation depends on the range of  $m_l$  variations. Hence the presence of strongly absorbing particles may increase the method's under-

tainties. In that context it should be pointed out that Böckmann<sup>10</sup> found that an increase in absorption leads to an increase in the degree of ill-posedness of the inverse problem, which in fact also points to increased retrieval uncertainty. The accuracy of the  $m_R$  estimation in the middle of the considered particle-size interval ( $r_0 \sim 0.7 \mu\text{m}$ ) is  $\pm 0.05$ , which agrees with the results from past sensitivity studies.<sup>8</sup> The realistic accuracy of the estimation of the imaginary part  $m_I$  is  $\pm 0.01$  in the present study. In the previous simulation studies we obtained 50% accuracy for  $m_I = 0.02$ , which again is in agreement.

(3) Simulation studies showed that the maximal mean particle size (for  $\ln \sigma = 0.4$ ), which may be estimated with an accuracy of better than 50%, is  $< 1 \mu\text{m}$ . The current analysis shows that the limit is  $\sim 1.5 \mu\text{m}$  for the mean particle size. These results are again in rather good agreement.

(4) The retrieval of the refractive index failed for small particles, while the particle size still could be estimated. The degradation of the accuracy of  $m_R$  retrieval from  $\pm 0.05$  to  $\pm 0.08$  with a decreasing mean radius from 1 to  $0.1 \mu\text{m}$  was also reported in our simulation studies.

(5) In the simulations and experiments carried out in the past we found that the microphysical parameters retrieved with  $3\beta + 2\alpha$  and  $6\beta + 2\alpha$  data sets do not differ too much.<sup>8,9,14</sup> This result may be understood from a current eigenvalue analysis showing that the information content of the spectra of particle backscatter and extinction coefficients is limited. As a result the sensitivities of  $3\beta + 2\alpha$  and  $6\beta + 2\alpha$  data sets are similar for the investigated particle parameters (effective radius, complex refractive index), if a 10% measurement error is considered. However, with a  $6\beta + 2\alpha$  data set the retrieval may become more robust with respect to measurement errors.

We also point out that the current analysis gives only rough estimations, so a comparison with the results from simulation studies should be done with care. The main advantage of this approach is the possibility of obtaining a more general picture and thus of understanding the way different parameters influence one another. The analysis was performed in rather idealized situations, but the approach may be extended to include the particles' bimodal size distribution, the size and wavelength dependence of the refractive index, and different types of kernel function used in retrieval and thus may provide motivation for targeted modifications of the inversion codes currently in use.

## References

1. A. N. Tikhonov and V. Y. Arsenin, eds., *Solution of Ill-Posed Problems* (Wiley, 1977).
2. S. Twomey, eds., *Introduction to the Mathematics of Inversion in Remote Sensing and Direct Measurements* (Elsevier, 1977).
3. V. E. Zuev and I. E. Naats, eds., *Inverse Problems of Lidar Sensing of the Atmosphere* (Springer-Verlag, 1983).
4. P. Qing, H. Nakane, Y. Sasano, and S. Kitamura, "Numerical simulation of the retrieval of aerosol size distribution from multiwavelength laser radar measurements," *Appl. Opt.* **28**, 5259–5265 (1989).
5. D. Müller, U. Wandinger, D. Althausen, I. Mattis, and A. Ansmann, "Retrieval of physical particle properties from lidar observations of extinction and backscatter at multiple wavelengths," *Appl. Opt.* **37**, 2260–2263 (1998).
6. D. Müller, U. Wandinger, and A. Ansmann, "Microphysical particle parameters from extinction and backscatter lidar data by inversion with regularization: theory," *Appl. Opt.* **38**, 2346–2357 (1999).
7. D. Müller, U. Wandinger, and A. Ansmann, "Microphysical particle parameters from extinction and backscatter lidar data by inversion with regularization: simulation," *Appl. Opt.* **38**, 2358–2368 (1999).
8. I. Veselovskii, A. Kolgotin, V. Griaznov, D. Müller, U. Wandinger, and D. N. Whiteman, "Inversion with regularization for the retrieval of tropospheric aerosol parameters from multiwavelength lidar sounding," *Appl. Opt.* **41**, 3685–3699 (2002).
9. I. Veselovskii, A. Kolgotin, V. Griaznov, D. Müller, K. Franke, and D. N. Whiteman, "Inversion of multiwavelength Raman lidar data for retrieval of bimodal aerosol size distribution," *Appl. Opt.* **43**, 1180–1195 (2004).
10. C. Böckmann, "Hybrid regularization method for ill-posed inversion of multiwavelength lidar data in the retrieval of aerosol size distributions," *Appl. Opt.* **40**, 1329–1342 (2001).
11. D. Müller, F. Wagner, D. Althausen, U. Wandinger, and A. Ansmann, "Physical properties of the Indian aerosol plume derived from six-wavelength lidar observation on 25 March 1999 of the Indian Ocean Experiment," *Geophys. Res. Lett.* **27**, 1403–1406 (2000).
12. D. Althausen, D. Müller, A. Ansmann, U. Wandinger, H. Hube, E. Clauder, and S. Zörner, "Scanning 6-wavelength 11-channel aerosol lidar," *J. Atmos. Ocean. Technol.* **17**, 1469–1482 (2000).
13. I. Mattis, A. Ansmann, D. Müller, U. Wandinger, and D. Althausen, "Multiyear aerosol observations with dual-wavelength Raman lidar in the framework of EARLINET," *J. Geophys. Res.* **109**, D13203, doi:10.1029/2004JD004600 (2004).
14. D. Müller, U. Wandinger, D. Althausen, and M. Fiebig, "Comprehensive particle characterization from three-wavelength Raman lidar observations: case study," *Appl. Opt.* **40**, 4863–4869 (2001).
15. C. L. Mateer, "On the information content of Umkehr observations," *J. Atmos. Sci.* **22**, 370–381 (1965).
16. A. Ben-David, B. M. Herman, and J. Reagan, "Inverse problem and the pseudoempirical orthogonal function method of solution. 1: Theory," *Appl. Opt.* **27**, 1235–1242 (1988).
17. D. P. Donovan and A. I. Carswell, "Principal component analysis applied to multiwavelength lidar aerosol backscatter and extinction measurements," *Appl. Opt.* **36**, 9406–9424 (1997).
18. M. J. Post, "A graphical technique for retrieving size distribution parameters from multiple measurements: visualization and error analysis," *J. Atmos. Ocean. Technol.* **13**, 863–873 (1996).
19. C. F. Bohren and D. R. Huffmann, *Absorption and Scattering of Light by Small Particles* (Wiley, 1983).